Geomechanics and Engineering, *Vol. 30, No. 4 (2022) 363-372*
https://doi.org/10.12989/gae.2022.30.4.363

Analytical behavior of longitudinal face dowels based on an innovative interpretation of the ground response curve method

Nima Rahimpour[1a], Morteza MohammadAlinejad Omran[2b] and Amir Bazrafshan Moghaddam*[2]

[1]*Faculty of Engineering, University of Tabriz, Tabriz, Iran*
[2]*Department of Civil Engineering, Shahrood University of Technology, Shahrood, Iran*

(*Received July 17, 2021, Revised July 12, 2022, Accepted July 24, 2022*)

Abstract. One of the most frequent issues in tunnel excavation is the collapse of rock blocks and the dropping of rock fragments from the tunnel face. The tunnel face can be reinforced using a number of techniques. One of the most popular and affordable solutions is the use of face longitudinal dowels, which has benefits including high strength, flexibility, and ease of cutting. In order to examine the reinforced face, this work shows the longitudinal deformation profile and ground response curve for a tunnel face. This approach is based on assumptions made during the analysis phase of problem solving. By knowing the tunnel face response and dowel behavior, the interaction of two elements can be solved. The rock element equation derived from the rock bolt method is combined with the dowel differential equation to solve the reinforced ground response curve (GRC). With a straightforward and accurate analytical equation, the new differential equation produces the reinforced displacement of the tunnel face at each stage of excavation. With simple equations and a less involved computational process, this approach offers quick and accurate solutions. The FLAC3D simulation has been compared with the suggested analytical approach. A logical error is apparent from the discrepancies between the two solutions. Each component of the equation's effect has also been described.

Keywords: analytical method; convergence confinement method; longitudinal dowels; tunnel face; weak rocks

1. Introduction

Weak rock is a major problem in tunnel excavation. The collapse of rock blocks, and falling of rock particles from the tunnel face and its perimeter are the main concerns. Various factors related to face stability have been investigated so far such as: Probabilistic analysis for face stability of tunnels in Hoek-Brown media (Li and Yang 2019), three-dimensional limit analysis of seismic stability of tunnel faces with quasi-static method (Zhang *et al*. 2021), the effect of non-circularity of a tunnel cross-section on the failure shape (Pan and Dias 2017), and the effect of geological conditions on the cone form of the failure zone (Senent *et al*. 2013).

The application of longitudinal fiberglass dowels is one of the most effective and conventional systems to solve the above-mentioned problem. Its advantages over other methods include its high strength, flexibility, and being easy to cut during the excavation. Furthermore, they are more efficient than forepoling elements in the reduction of face deformation. These elements reinforce the tunnel face by establishing an adherence between the dowel and surrounding soil by cement grout and apply a confining pressure on the critical failure zone. This new united zone reduces the plastic zone behind the face (Yoo and Geotechnics 2002).

Since 2000, numerous studies have been conducted to examine the problem of excavation face stability in deep tunnels in the presence of fiberglass reinforcements by numerical methods (e.g., Chen, Zou *et al*. 2019) and by simplified analytical methods (e.g., Dias 2011, Oreste 2013) Most analytical attempts have been based on the homogenization method, which simulates both dowels and rock at the tunnel face as an equivalent material.

Although previous investigations address the mechanical behavior of dowels, they could not accurately calculate the maximum tensile force of dowels. Dias (2011) employed the convergence confinement method (CCM) to secure the maximum displacement of the face. A new interpretation of the ground response curve (GRC) was used for the tunnel face, and the concepts of support characteristic curve for dowels, in the absence or presence of grout, were utilized. This study presented a simple method to evaluate face stability, disregarding the interaction mechanism between the dowels' element and the surrounding rock. As dowels reinforce the weak rock, their behavior is not independent of the rock; therefore, dowels and rock displacements cannot be separated.

Oreste (2013) analyzed deep tunnel face failure by the limit method and presented an explicit procedure based on the finite-difference approach for analyzing the presence of dowels in the rock mass. The dowels were considered distinctly through the shear stresses applied to the dowel–rock interface.

*Corresponding author, Assistant Professor
E-mail: amir.bazrafshan@shahroodut.ac.ir;
amir.bazrafshan@gmail.com
[a]Graduated Student
[b]Post Graduate Student

ISSN: 2005-307X (Print), 2092-6219 (Online)

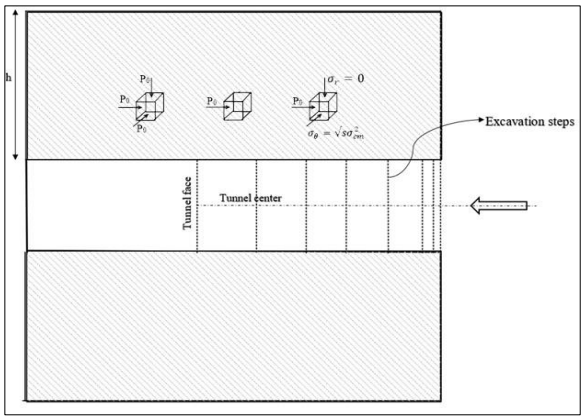

Fig. 1 Tunnel excavation and wall active pressures

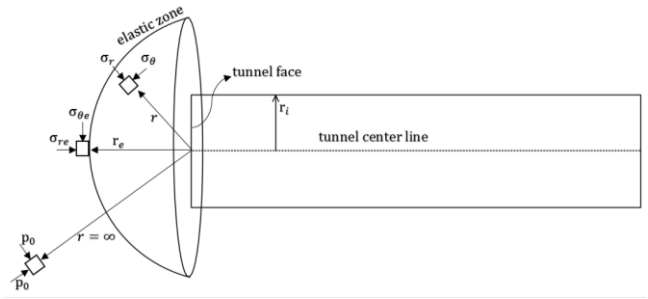

Fig. 2 Different stress positions around the excavated tunnel face

All these studies have facilitated the examination of the role and action mechanisms of fiberglass reinforcements in the stability of the excavation face. However, in order to achieve a proper dimensioning, three-dimensional numerical simulations are challenging. Additionally, analytical approaches are either based on unduly simplistic assumptions or the homogenization method.

Therefore, this study presents a new analytical method to calculate the displacements of the reinforced tunnel face. It provides the most effective estimation of the supporter of the tunnel face to start three-dimensional numerical simulations of the problem with fewer iterations. It is assumed that the dowels' effect is combined with the convergence confinement equations to increase the strength of the rock. To this end, the differential equation of the dowel face is added to the rock media. A modified differential equation with the addition of the effect of dowels is solved. The results show that the GRC of the reinforced face is converged faster than the unreinforced face.

In addition, the differential equations are modified from the rock bolt equations because of the hydrostatic conditions. Bolts are not utilized in face dowels because they have an unreal influence on the rock bolt equation and reinforced tunnel wall differential equations. This is because the behavioral mechanism of rock bolts differs slightly from that of dowels. As a result, it is possible to deduce the differential equations for the tunnel face from the equations for the tunnel's reinforced wall. The tunnel wall is referred to in the ground response curve of tunnels here. The new behavior of GRC as it relates to the hydrostatic condition is identified by this study. As a result, the reinforced tunnel face GRC technique and the new differential equation are combined to provide the final displacements.

2. The proposed analytical simulation

2.1 Problem definition and assumptions

The GRC method has been introduced in accordance with the tunnel wall behavior in different rock mass specifications (Hoek 2001, Hoek 2018) and some studies have been conducted to modify it. These studies present the displacement of the tunnel wall accurately and consider an almost real rock behavior (elastoplastic in hydrostatic conditions) (Wang 1996, Alonso *et al*. 2003, Lee and Pietruszczak 2008).

A circular tunnel with radius r_j is driven in a homogeneous and isotropic medium initially subjected to hydrostatic pressure P_0. As the full-face excavation advances, tunnel wall radial displacement occurs, and the in-situ stress starts to redistribute in the cross-section of the tunnel. Fig. 1 illustrates the process of stresses' redistribution around the excavation in different sections.

As shown in Fig. 1, the stresses have been redistributed and altered in different cross-sections in front of the tunnel face where the longitudinal stress remains stable (this is provable by an assumption of plane strain condition). As the tunnel is excavated, the radial and tangential stresses are reduced, but stress remains constant in the direction of the tunnel axis.

At a distance away from the face of the tunnel, the value of stress in all directions is P_0. Close to the face, however, the stresses are redistributed and altered due to face displacements. The shorter the distance from the tunnel face, the more the inward displacements and redistribution of stresses.

The spherical symmetry hypothesis is used to analyze the redistribution of stress behind a deep tunnel's face (Fig. 2), i.e., the tunnel's cylindrical form with radius r_i and the distance between its face and specific zones as a hemispherical void with radius r. The stresses and strains around the cavity are calculated if the hydrostatic pressure P_0 is originally applied to this void. The tunnel face behavior in this case matches to those of a tunnel wall (Fig. 2).

As tunnel excavation advances, the longitudinal stress decreases in the target point, and the corresponding displacement occurs. When the face reaches the target point, the amount of stress tends to zero, and maximum displacement occurs. Therefore, the CCM can be used to calculate tunnel face displacement, and particularly, GRC can predict the extrusion of the tunnel face. Then, the stress is diminished from its initial value P_0 (point III in Fig. 3).

The following assumptions are also made:

- The value of the radial displacements on the surface of the sphere is an estimation of the mean extrusion displacement of the excavation face.
- The excessive stress values developed by tunnel

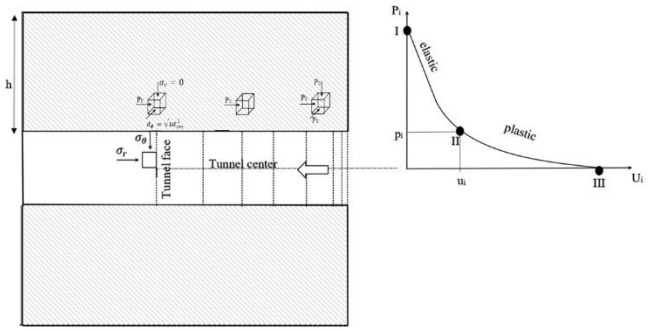

Fig. 3 Tunnel excavation and face active pressures

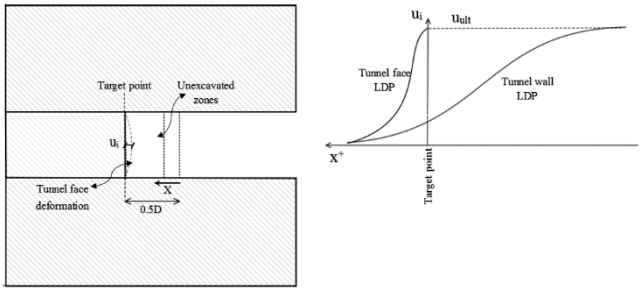

Fig. 4 Schematic representation of the modified LDP of the tunnel face

supports, close to the excavation face, are negligible.

Fig. 4 displays the longitudinal deformation profile (LDP) of the tunnel face, which is similar to the LDP of the tunnel wall. As the excavation face approaches the target point, the displacements increase and finally reach their maximum value when the excavation face reaches the target point. This process, i.e., the extrusion displacements of the target point behind the tunnel face, starts when the face approaches the distance of 0.5 D (where D is the tunnel diameter). For the tunnel wall, it starts when the distance of the tunnel face is between 0.5D and 1.5D. The LDP of the tunnel face increases to ultimate displacement in a short distance (0.5 D). Fig. 5 illustrates the behavior of the LDP as well as GRC. The GRC of the tunnel in this study was developed using Park's method (Park *et al*. 2008).

2.2 Analytical simulation of the longitudinal dowels

This section presents the analytical simulation of the fully-grouted longitudinal dowels.

2.2.1 Ideal connection

As previously indicated, tunnel deformation for the tunnel wall under hydrostatic conditions is identical in all directions and angles to a standard GRC. As a result, the tunnel wall's face dowel reinforcement behaves in the same way as its radial reinforcements (rock bolts). When utilizing a face dowel, the dowel contribution is made in the form of an even load distribution throughout the tunnel face, and each dowel has an impact on a specific area of the zone.

Therefore, the differential equation of equilibrium for the tunnel face with a circular cross-section, hydrostatic stress conditions, and close spacing of the face-dowels will be based on (Fahimifar and Soroush 2005). The following is

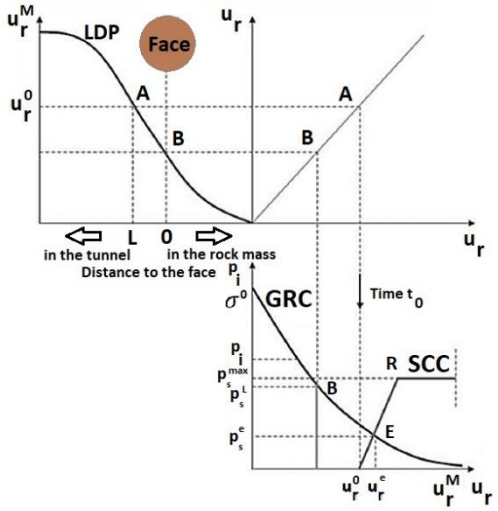

Fig. 5 LDP and GRC of the tunnel

a modified differential equation for the tunnel face under hydrostatic conditions (see Eqs. (1) and (2)).

$$\frac{\mathrm{d}\sigma_r'}{\mathrm{d}r} = \frac{\sigma_\theta - \sigma_r'}{r} \tag{1}$$

$$\sigma_r' = \sigma_r - \frac{T}{C} \tag{2}$$

where σ_r is the adjusted radial stress in the rock mass. In Eq. (2), the tunnel rock mass is strengthened with the addition of the dowels. Eq. (2) increases the virtual rock specification, so tunnel displacement convergence is faster than usual. Furthermore,σ_θ is the tangential stress; r is a variable denoting the distance from the tunnel face, and T is the overall face dowel tensional force. If the tunnel face convergence does not increase, then the force along the dowel be almost constant and equal to zero (i.e., T=0). Thus, *dT/dr* will be equal to zero, and the following equation can be written based on Eq. (1) (by replacing the Hoek–Brown strength criterion, see Eq. (3) (Brown and Hoek 1980)). Here, σ_c is the uniaxial compressive strength of the intact rock material, and parameters$\bar{s}$and$\bar{m}$are rock mass constants, depending on the rock and its geotechnical conditions.

$$\frac{\mathrm{d}\sigma_r}{\mathrm{d}r} = \frac{[\bar{m}\sigma_c\sigma_r + \bar{s}\sigma_c^2]^{\frac{1}{2}}}{r} \tag{3}$$

where

$$\sigma_\theta = \sigma_r + \left(\bar{m}\sigma_r\sigma_c + \bar{s}\,\sigma_c^2\right)^{\frac{1}{2}} \rightarrow \bar{m} = m_p, \bar{s} = s_p \tag{4}$$

According to the rock behavior, the tunnel boundary condition can be determined as

1. At $r = r_i$ $(L = 0) \rightarrow$ $\sigma_r = p_i$ in which $0 \le p_i \le p_0$(because the face dowel increases the strength of the tunnel face specification) (Fig. 6).
2. At $r = r_e$ $(L = L_e) \rightarrow$ $\sigma_r = \sigma_{re}$

Here, p_i is the longitudinal pressure in the tunnel face; σ_{re} is the radial stress (normal to the tunnel face boundary) and is obtained at the outer boundary of the plastic zone. A

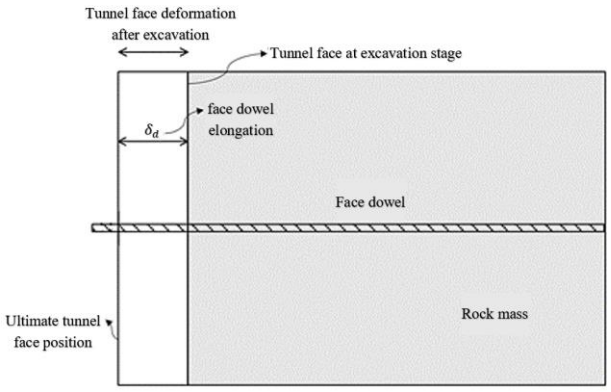

Fig. 6 Modification in the elastic part of the model, tunnel face, and dowel displacement

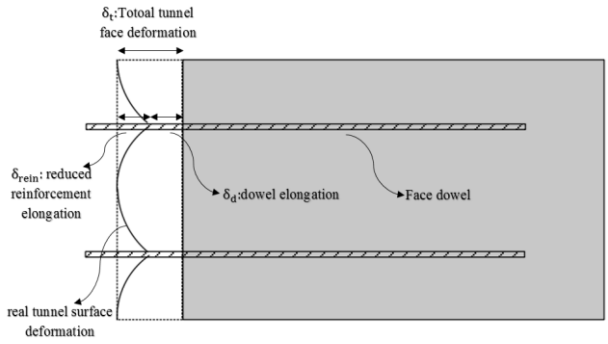

Fig. 7 Real behavior of the dowel and tunnel face displacement

common application of face dowels is in weak and weathered rock mass, so the behavior of rock under excavation is considered perfectly plastic.

Decreasing the radial pressure on the tunnel face from its remaining value (by excavation) raises the tunnel face deformations and imposes further tension on the dowels. Thus, the differential equation for this condition will be rewritten according to Eq. (3), and the dowel force is obtained by Eq. (5).

$$T = A_d.E_d.\varepsilon_d \tag{5}$$

where A_d, E_d and ε_d, are the dowel's cross-sectional area, the modulus of elasticity, and dowel axial strain (which is equal to tunnel face deformation (this section's assumption)), respectively. Tunnel and dowel deformation are schematically illustrated in Fig. 6.

Elastic part

Theoretically, face dowel stabilization is installed prior to the excavation process and, thus, the elastic behavior of the reinforced zone must be modified. The radial and tangential elastic stresses are obtained based on

$$\sigma_{r1} = \sigma_{re} = p_0 - M\sigma_c \ , \sigma_{\theta 1} = \sigma_{\theta e} = 2p_0 - \sigma_{r1} \tag{6}$$

Moreover, the radial and tangential elastic strains are obtained based on

$$\varepsilon_{\theta 1} = \varepsilon_{\theta 1}^{e} = \varepsilon_{\theta e} = \left(\frac{1}{2G}\right)[(1-\vartheta)(\sigma_{\theta 1} - p_0) - \vartheta(\sigma_{r1} - p_0)] \tag{7}$$

$$\varepsilon_{r1} = \varepsilon_{r1}^{e} = \varepsilon_{re} = \left(\frac{1}{2G}\right)[(1-\vartheta)(\sigma_{r1} - p_0) - \vartheta(\sigma_{\theta 1} - p_0)] \tag{8}$$

Within the elastic part, as the tunnel face deforms, the dowel elongation increases. For simplification, the face dowel force can be assumed as Eq. (9)

$$T = E_d A_d \varepsilon_{re} \tag{9}$$

This force can be transformed to the virtual radial stress and strengthen the radial stress of the tunnel face (Eq. (10)).

$$\sigma_{r\_d} = \frac{T}{c} \quad \rightarrow \quad \sigma_{r1(\text{modified})} = \sigma_{r1} - \sigma_{r\_d} \tag{10}$$

According to Eq. (6), tangential stress is recalculated as

$$\sigma_{\theta 1(\text{modified})} = 2p_0 - \sigma_{r1(\text{modified})} \tag{11}$$

Therefore, radial and tangential strains are

$$\begin{cases} \varepsilon_{r1} = \varepsilon_{r1}^{e} = \varepsilon_{r1(\text{modified})}^{e} = \left(\frac{1}{2G}\right)\left[(1-\vartheta)\left(\sigma_{r1(\text{modified})} - p_0\right) - \vartheta\left(\sigma_{\theta 1(\text{modified})} - p_0\right)\right] \\ \varepsilon_{\theta 1} = \varepsilon_{\theta 1}^{e} = \sigma_{\theta 1(\text{modified})} = \left(\frac{1}{2G}\right)\left[(1-\vartheta)\left(\sigma_{\theta 1(\text{modified})} - p_0\right) - \vartheta\left(\sigma_{r1(\text{modified})} - p_0\right)\right] \end{cases} \tag{12}$$

Plastic part

To solve differential Eqs. (1) and (3), it is necessary to employ a numerical method given their algebraic nature. Brown *et al*. (1983) applied a semi-analytical (analytical-numerical) approach, including the dowel parameters, to calculate the stresses and strains around a reinforced circular tunnel face. This method is an iterative finite-difference solution. Therefore, the modified differential Eq. (1) is rewritten for a loop. Eqs. (13) and (14) have been obtained based on (Fahimifar and Soroush 2005)

$$\frac{d\sigma_r}{dr} = \frac{\left[m_r\sigma_c\left(\sigma_r - \frac{T}{c}\right) + s_r\sigma_c^2\right]^{\frac{1}{2}} - \frac{T}{c}}{r} \tag{13}$$

where Eq. (13) is obtained by the substitution of Eq. (14).

$$\sigma_\theta - \sigma_r = \left[m_p\sigma_c\left(\sigma_r - \frac{T}{c}\right) + s_r\sigma_c^2\right]^{\frac{1}{2}} - \frac{T}{c} \tag{14}$$

Decomposing Eq. (13) gives

$$\frac{\sigma_{r(J-1)} - \sigma_{r(J)}}{r_{(J-1)} - r_J} = \left[\frac{m_a\sigma_c}{2}\left[\left(\sigma_{r(J)} + \sigma_{r(J-1)}\right) - \frac{T_{(J)} + T_{(J-1)}}{C}\right] + s_a\sigma_c^2\right]^{\left(\frac{1}{2}\right)} - \left[\frac{T_{(J)} + T_{(J-1)}}{2C}\right] \times \frac{2}{r_J + r_{(J-1)}} \tag{15}$$

where

$$T_{(J)} = E_d A_d \varepsilon_{r(J)} \tag{16}$$

Eq. (17) gives the radial stress of the tunnel face in each step, obtained with some elaboration on Eq. (15).

$$\sigma_{r(J)} = \frac{-b - \sqrt{b^2 - 4ac}}{2a} \tag{17}$$

where

$$a = \frac{1}{4k^2} \ . \ b = \frac{-k_1}{k} - \frac{\sigma_{r(J-1)}}{2k^2} - 2k_2$$

$$c = \left(\frac{\sigma_{r(J-1)}^2}{4k^2} + k_1^2 + \frac{k_1}{k}\sigma_{r(J-1)} - 2k_2\sigma_{r(J)} + 4k_1k_2 - s_a\sigma_c^2\right)$$

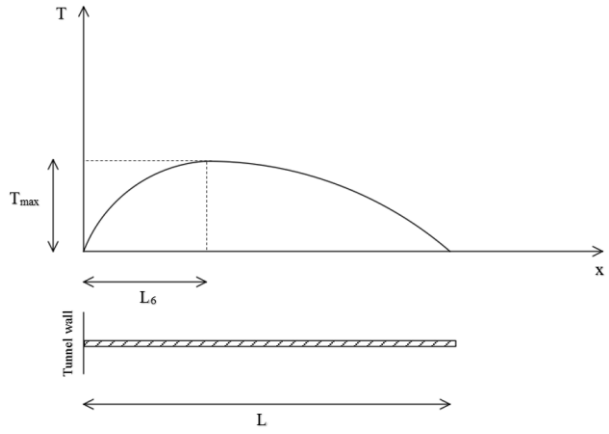

Fig. 8 Dowel force distribution along the face dowel

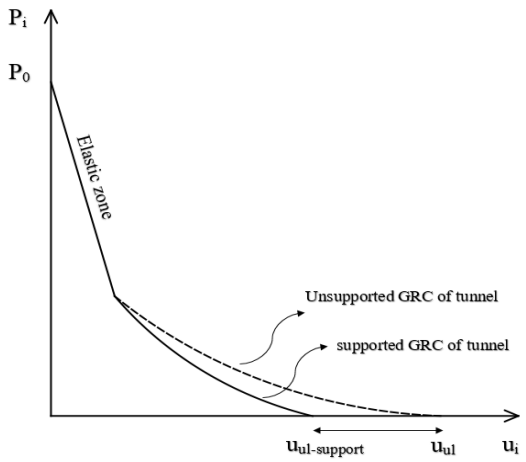

Fig. 9 Final displacement of the reinforced and unreinforced tunnel face

To find the parameters of the roots of the equation, refer to Appendix I.

2.2.2 Shear displacement between the bolt and rock mass

Fig. 7 shows the real behavior of the rock reinforced with face dowels. It can be observed that the minimum deformation happens around the dowel rock, while the maximum deformation occurs between the dowels.

It can be modified by Eq. (18), proposed based on (Fahimifar and Soroush 2005). Nevertheless, the initial conditions have been obtained according to the behavior of the tunnel face and dowels.

$$T_{\text{modified}} = T_{\text{ideal}} - \left[-T_{\max}\left(\frac{e^{-\lambda \text{L}}}{e^{\lambda \text{L}}+e^{-\lambda \text{L}}}\right)\left(e^{\lambda \text{x}} + e^{2\lambda \text{L}}e^{-\lambda \text{x}}\right)\right] \quad (18)$$

In sequence of the tunnel convergence calculation, Eq. (18) is rewritten as

$$T_{(j)} = T_{\text{ideal}(j)} - \left[-T_{\text{ideal}(j)}\left(\frac{e^{-\lambda \text{L}}}{e^{\lambda \text{L}}+e^{-\lambda \text{L}}}\right)\left(e^{\lambda(r_j-r_i)} + e^{2\lambda \text{L}}e^{-\lambda(r_j-r_i)}\right)\right] \quad (19)$$

$T_{ideal\ (j)}$ is calculated based on Eq. (20), and the force distribution along the dowel has been shown in Fig. 8.

$$T_{\text{ideal}(j)} = E_d A_d \varepsilon_{r(J)} \quad (20)$$

Substituting Eq. (19) into Eq. (15) yields

$$T_{(J)} = E_d A_d \varepsilon_{r(J)} - \left[-E_d A_d \varepsilon_{r(J)}(1-\beta)\left(\frac{e^{-\lambda \text{L}}}{e^{\lambda \text{L}}+e^{-\lambda \text{L}}}\right)\left(e^{\lambda(r_j-r_i)} + e^{2\lambda \text{L}}e^{-\lambda(r_j-r_i)}\right)\right] \quad (21)$$

According to the Eq. (15) and same as the first part of equations

$$a = \frac{1}{4k^2}.\ \text{b} = \frac{-k_1}{k} - \frac{\sigma_{r(J-1)}}{2k^2} - 2k_2\ .$$

$$c = \left(\frac{\sigma_{r(J-1)}^2}{4k^2} + k_1^2 + \frac{k_1}{k}\,\sigma_{r(J-1)} - 2k_2\sigma_{r(J)} + 4k_1k_2 - s_a\sigma_c^2\right)$$

and

$$k_1 = \frac{(E_d A_d Coef)}{2C} - [-E_d A_d \varepsilon_{r(j)}\left(\frac{(e^{-\lambda L})}{(e^{\lambda^L}+e^{-\lambda L})}\right)(e^{\lambda(r_j-r_i)} + e^{2\lambda L}e^{-\lambda(r_j-r_i)})$$

Table 1 The specifications of different supporting systems

Supporting system specifications	Face dowels
Young's modulus (GPa)	40
Cross-section (m^2)	$15.708\times10^{(-4)}$
Tension yield strength (Pa)	∞
Grout stiffness (Pa)	10×10^9
Dowel young's modulus (GPa)	45

Table 2 Analytical and numerical magnitude of the face displacement in different rock specifications (r=5 m)

GSI	P_0	Supporting system	Displacement (numerical)	Displacement (proposed method)	Error
15	2	Dowel	0.95	1.07	11.12
	4	Dowel	2.44	2.25	8.3
	8	Dowel	5.52	5.11	7.42
20	2	Dowel	0.73	0.81	9.87
	4	Dowel	1.79	1.72	4.1
	8	Dowel	4.13	3.86	7
30	2	Dowel	0.42	0.46	8.7
	4	Dowel	1.03	0.97	6.2
	8	Dowel	2.28	2.16	5.55

(System units: MPa, cm, percent (%))

The other parameters remain constant.

Based on Fig. 9, the ratio of the supported tunnel displacement and ultimate unsupported tunnel displacement is indicated by the ψ parameter. Multiplying this parameter by the unsupported displacements yields the supported displacement of the tunnel face. The ψ parameter is defined as (Ranjbarnia, Rahimpour *et al*. 2018)

$$\psi = \frac{U_{ul}-Support}{U_{ul}} \quad (22)$$

3. Results

Table 1 presents the specifications of the structural elements used in this study. These parameters are the current inputs of FLAC^{3D} based on real structures.

Table 3 Analytical and numerical magnitude of the face displacement in different rock specifications (r=3 m)

GSI	P_0	Supporting system	Displacement (numerical)	Displacement (proposed method)	error
15	2	Dowel	0.59	0.64	7.8
	4	Dowel	1.44	1.35	6.67
	8	Dowel	3.27	3.07	6.5
20	2	Dowel	0.44	0.48	8.3
	4	Dowel	1.01	1.03	1.9
	8	Dowel	2.48	2.31	7.35
30	2	Dowel	0.25	0.27	8
	4	Dowel	0.53	0.58	8.6
	8	Dowel	1.39	1.3	6.9

(System units: MPa, cm, percent (%))

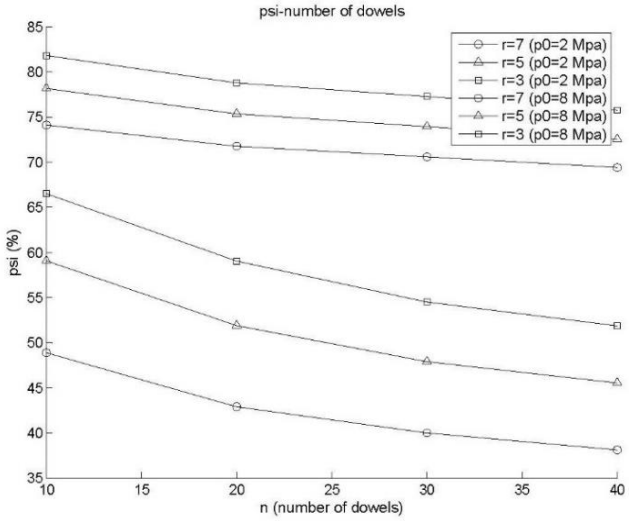

Fig. 10 The effect of the number of dowels on ψ

Because this reinforcing system is used on weak rock; the rock specification is considered in the category of weak rock (Hoek 2001, 2018). Here, rock behaves as a perfect plastic. Therefore, there is no need to model the strain softening behavior in FLAC3D software. Hence, modified Hoek and Brown (Hoekbrown) is selected in FLAC3D; and face dowels were modeled as cables in the software. Grout stiffness is the interface springs for modeling the boundary between the rock and dowel. According to the software manual's recommendations, this parameter must be considered a large number.

Tables 2 and 3 compare the result of numerical and proposed analytical displacements in different rock mass qualifications and in the presence of the face supporting systems.

A comparison of the results shows an acceptable correlation and negligible errors between the numerical and proposed analytical methods. In the following sections, the effect of each parameter of formula with more details have been analyzed to show the effect of each. Different number of dowels, dowel stiffness, rock specifications and tunnel depth (hydrostatic pressure) are the effective parameters and the influence of each one has been discussed. These results will lead to optimal analysis.

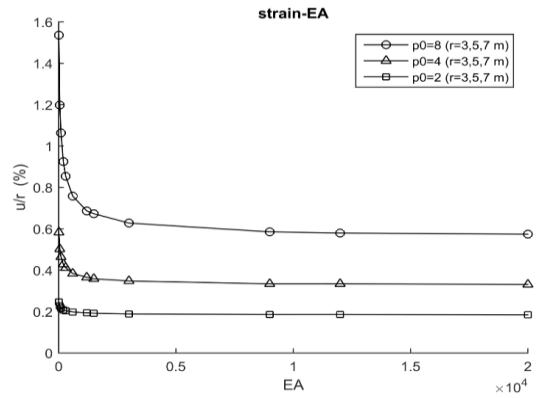

Fig. 11 The effect of supporting system stiffness on tunnel face strain

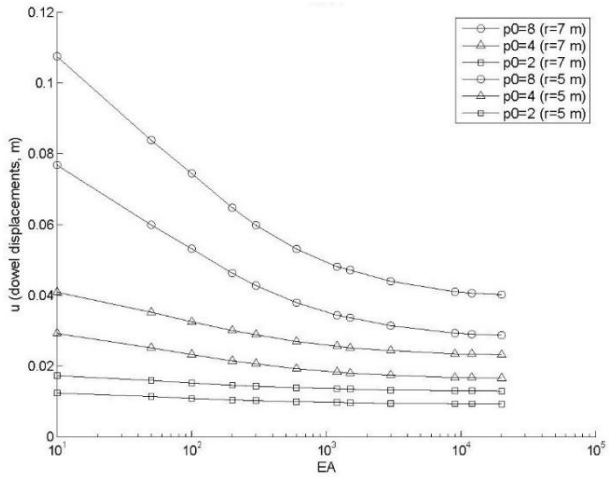

Fig. 12 The effect of supporting system stiffness on dowel displacement

3.1 The effect of the number of the dowels on ψ parameter

Number of dowels is one of the important parameters to reduce tunnel face deformation. According to Eq. (15), this parameter causes an increase in the reinforced area of tunnel face and reduces face deformations.

Different numbers of dowels have been applied in the tunnel face to identify the reinforced displacement and its rate. According to Fig. 10, as the number of dowels increases, the ψ parameter decreases. Dowel numbers more than 30 have no effect on the ψ parameter.

3.2 Stiffness of the dowels

Based on the Eq. (15), stiffness of the dowels has direct effect on tunnel face deformation. Therefore, it is essential to know the rate of dowel stiffness effect on tunnel reinforcement. Dowel stiffness is defined as a function of the module of elasticity and cross-sectional area. Figs. 11 and 12 illustrate the effect of dowels and grout specification on the strain of the tunnel face in different tunnel radii and stress fields. Parameters E and A are the elasticity modulus and area of the dowel, respectively.

The gradient of the stiffness becomes smoother

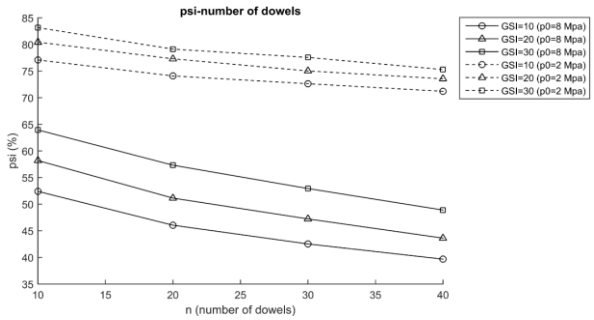

Fig. 13 Different rock specifications on tunnel face ψ

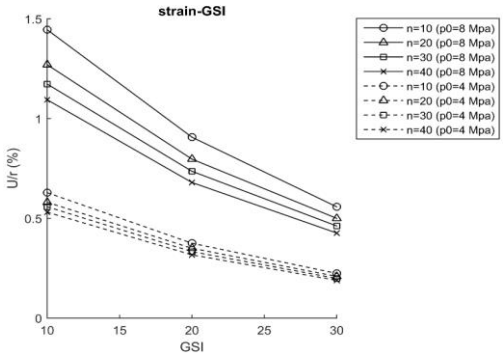

Fig. 14 The effect of various rock GSI on tunnel face strain

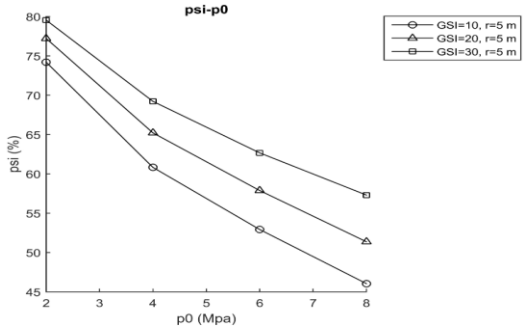

Fig. 15 The effect of tunnel depth on tunnel face ψ

considering EA>3000. In addition, EA>9000 has no more effect on the ψ (tunnel face displacement reduction) parameter. It can be concluded that the efficiency of the supporting system stiffness is greater at deeper depths.

3.3 The effect of the number of dowels on ψ parameter in different rock mass specifications (GRC)

This section demonstrates the effect of tunnel depth and the number of dowels in various rock geological conditions (GSI=10, 20 and 30). Fig. 13 indicates the effect of rock specification on tunnel face ψ. Evidently, the supporting systems are more effective in weak rocks.

Increasing the number of dowels is more useful in weak rocks. Based on Fig. 13, applying fewer dowels in weak rock (GSI=10) is more effective than applying more dowels in a relatively strong rock (GSI=30).

According to Fig. 14, increasing the tunnel rock specification (GSI) would reduce the tunnel face strain. For the GSI>25, it may be assumed that no noticeable changes have taken place.

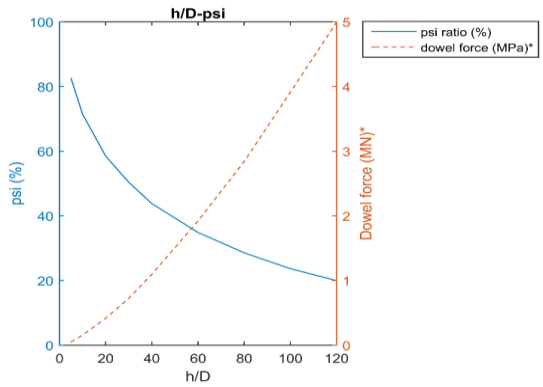

Fig. 16 The effect of h/D parameter on tunnel face ψ and dowel force

3.4 Effect of tunnel depth on the ψ ratio

According to Fig. 15, the ψ parameter decreases by increasing the tunnel depth. Thus, it can be concluded that dowels are more effective in deeper tunnels. Different GSIs in shallow tunnels have almost the same ψ.

3.5 The effect of h/D parameter on ψ ratio and dowels' force

Fig. 16 illustrates the effect of the ψ parameter against the variation of the h/D ratio. Moreover, dowels' force increases with raising the tunnel face strain, which has been shown in the second vertical axis of Fig. 16.

It can be concluded that, this reinforcement is more efficient in deep tunnels or tunnel with high hydrostatic pressure.

4. Conclusions

Face dowels are one of the most efficient pre-reinforcement methods for stabilizing the tunnel face in weak rock. The mechanism of the longitudinal face dowel consists of stabilizing the tunnel face in falling zones.

Based on the suggested GRC approach, this study examined various rock and dowel specifications in tunnel face deformation. According to the findings, the supporting structure lessens the load on the tunnel face. Additionally, it is effective to apply grout around the dowel. The CCM helps analyze the reinforced face. The mechanism of the dowels is based on tensile elements. Consequently, longitudinal stiffness is an important factor for designing the reinforcement elements. The presented equations showed the effect of each parameter on tunnel face displacement. The findings show that the main parameters, which are more effective in weak rocks and deep excavations, are the number of the dowels and their stiffness.

With a high degree of precision, this technique can simulate tunnel face behavior under various conditions. However, because this approach is analytical, it cannot be used with other tunnel reinforcement techniques (due to the complexity of differential equations). Therefore, a

comprehensive analytical study that would calculate the exact value of displacements is subject to large error. It will be difficult for the tunnel face displacement to occur when reinforced with dowels considering the tunnel wall support. The specification of the reinforcements is primarily determined by analytical approaches with the least amount of iteration.

References

Alonso, E., Alejano, L., Varas, F., Fdez-Manin, G. and Carranza-Torres, C. (2003), "Ground response curves for rock masses exhibiting strain-softening behaviour", *Int. J. Numer. Anal. Meth. Geomech.*, **27**(13), 1153-1185. https://doi.org/10.1002/nag.315.

Brown, E. and Hoek, E. (1980), *Underground Excavations in Rock*, CRC Press.

Brown, E.T., Bray, J.W., Ladanyi, B. and Hoek, E. (1983), "Ground response curves for rock tunnels", *J. Geotech. Eng.*, **109**(1), 15-39. https://doi.org/10.1061/(ASCE)0733-9410(1983)109:1(15).

Cai, Y., Esaki, T. and Jiang, Y. (2004), "A rock bolt and rock mass interaction model", *Int. J. Rock Mech. Min. Sci.*, **41**(7), 1055-1067. https://doi.org/10.1016/j.ijrmms.2004.04.005.

Chen, G.H., Zou, J.F. and Qian, Z.H. (2019), "An improved collapse analysis mechanism for the face stability of shield tunnel in layered soils", *Geomech. Eng.*, **17**(1), 97-107. https://doi.org/10.12989/gae.2019.17.1.097.

Dias, D. (2011), "Convergence-confinement approach for designing tunnel face reinforcement by horizontal bolting", *Tunnel. Underg. Space Technol.*, **26**(4), 517-523. https://doi.org/10.1016/j.tust.2011.03.004.

Fahimifar, A. and Soroush, H. (2005), "A theoretical approach for analysis of the interaction between grouted rockbolts and rock masses", *Tunnel. Underg. Space Technol.*, **20**(4), 333-343. https://doi.org/10.1016/j.tust.2004.12.005.

Hoek, E. (2001), "Rock mass properties for underground mines", *Underground Mining Methods: Engineering Fundamentals And International Case Studies*, **21**.

Hoek, E. (2018), *Support for Very Weak Rock Associated with Faults and Shear Zones*, Routledge.

Lee, Y.K. and Pietruszczak, S. (2008), "A new numerical procedure for elasto-plastic analysis of a circular opening excavated in a strain-softening rock mass", *Tunnel. Underg. Space Technol.*, **23**(5), 588-599. https://doi.org/10.1016/j.tust.2007.11.002.

Li, T. and Yang, X. (2019), "Probabilistic analysis for face stability of tunnels in Hoek-Brown media", *Geomech. Eng.*, **18**(6), 595-603. https://doi.org/10.12989/gae.2019.18.6.595.

Oreste, P. (2013), "Face stabilization of deep tunnels using longitudinal fibreglass dowels", *Int. J. Rock Mech. Min. Sci.*, **58**, 127-140. https://doi.org/10.1016/j.ijrmms.2012.07.011.

Pan, Q. and Dias, D. (2017), "Safety factor assessment of a tunnel face reinforced by horizontal dowels", *Eng. Struct.*, **142**, 56-66. https://doi.org/10.1016/j.engstruct.2017.03.056.

Park, K.H., Tontavanich, B. and Lee, J.G. (2008), "A simple procedure for ground response curve of circular tunnel in elastic-strain softening rock masses", *Tunnel. Underg. Space Technol.*, **23**(2), 151-159. https://doi.org/10.1016/j.tust.2007.03.002.

Ranjbarnia, M., Rahimpour, N. and Oreste, P. (2018), "A simple analytical approach to simulate the arch umbrella supporting system in deep tunnels based on convergence confinement method", *Tunnel. Underg. Space Technol.*, **82**, 39-49. https://doi.org/10.1016/j.tust.2018.07.033.

Senent, S., Mollon, G. and Jimenez, R. (2013), "Tunnel face stability in heavily fractured rock masses that follow the Hoek–Brown failure criterion", *Int. J. Rock Mech. Min. Sci.*, **60**, 440-451. https://doi.org/10.1016/j.ijrmms.2013.01.004.

Wang, Y. (1996), "Ground response of circular tunnel in poorly consolidated rock", *J. Geotech. Eng.*, **122**(9), 703-708. https://doi.org/10.1061/(ASCE)0733-9410(1996)122:9(703).

Yoo, C.J.C. and Geotechnics (2002), "Finite-element analysis of tunnel face reinforced by longitudinal pipes", *Comput. Geotech.*, **29**(1), 73-94. https://doi.org/10.1016/S0266-352X(01)00020-9.

Zhang, B., Jiang, J., Zhang, D.B. and Liu, Z. (2021), "Upper bound solution of collapse pressure and permanent displacement of 3D tunnel faces using the pseudo-dynamic method and the kinematic approach", *Geomech. Eng.*, **25**(6), 521-533. https://doi.org/10.12989/gae.2021.25.6.521.

CC

Notations

CCM	Convergence confinement method
GRC	Ground response curve
SCC	Support characteristic curve
LDP	Longitudinal deformation profile of tunnel
D	Tunnel diameter
r	Tunnel radius
$\sigma_{r(j)}$	Radial stress in (j)th iteration
$\bar{m}_j$	Rock specification in (j)th iteration
$\bar{s}_j$	Rock specification in (j)th iteration
σ_c	intact rock strength
p_i	Virtual tunnel wall and face pressure in (i)th st
p_0	Initial stress (in-situ stress)
u_i	Tunnel wall and face displacement in (i)th step
σ_θ	Tangential stress around the excavated zone
T	Dowel force
C	Area of dowel
r_e	Elastic radius of tunnel wall
ε_r	radial strain
$\varepsilon_{\theta(j)}$	Tangential strain in (j)th iteration
λ_j	Parameter of displacement in (j)th iteration
A_d	Area of dowel
E_d	Module of elasticity
ε_d	Dowel strain
T_{ideal}	Dowel force in ideal connection
$T_{modified}$	Dowel force in modified connection (shear simulation)
a,b,c	The parameter of second order equation
GSI	Rock strength specification
n	Number of dowels
$\psi\ (psi)$	Ratio of supported and unsupported ultimate displacement of tunnel face
$U_{ul-support}$	Ultimate displacement of the reinforced tunnel face
U_{ul}	Ultimate displacement of the unreinforced tunnel face

Appendix I

$$\sigma_\theta - \sigma_r = \left[m_r\sigma_c\left(\sigma_r - \frac{T}{c}\right) + s_r\sigma_c^2\right]^{\frac{1}{2}} - \frac{T}{c} \quad \text{(I-1)}$$

$$\frac{\mathrm{d}\sigma_r}{\mathrm{dr}} + \frac{\sigma_r - \sigma_\theta}{r} = 0 \quad \text{(I-2)}$$

With substituting (I-1) to (I-2)

$$\frac{\mathrm{d}\sigma_r}{\mathrm{dr}} = \frac{\left[m_r\sigma_c\left(\sigma_r - \frac{T}{c}\right) + s_r\sigma_c^2\right]^{\frac{1}{2}} - \frac{T}{c}}{r} \quad \text{(I-3)}$$

Decomposing the Eq. (I-3) gives

$$\frac{\sigma_{r(J-1)} - \sigma_{r(J)}}{r_{(J-1)} - r_J} = \left[\frac{m_a\sigma_c}{2}\left[\left(\sigma_{r(J)} + \sigma_{r(J-1)}\right) - \frac{T_{(J)} + T_{(J-1)}}{C}\right] + s_a\sigma_c^2\right]^{\left(\frac{1}{2}\right)} - \left[\frac{T_{(J)} + T_{(J-1)}}{2C}\right] \times \frac{2}{r_J + r_{(J-1)}} \quad \text{(I-4)}$$

Dowel force in Eq. (I-4) can be replaced with Eq. (I-5)

$$T_{(J)} = E_d A_d \varepsilon_{r(J)} \quad \text{(I-5)}$$

then

$$\frac{\sigma_{r(J-1)} - \sigma_{r(J)}}{r_{(J-1)} - r_J} = \left[\frac{m_a\sigma_c}{2}\left[\left(\sigma_{r(J)} + \sigma_{r(J-1)}\right) - \frac{E_d A_d}{C}\left(\varepsilon_{r(J)} + \varepsilon_{r(J-1)}\right)\right] + s_a\sigma_c^2\right]^{\frac{1}{2}} - \frac{A_d\varepsilon_d}{c} \times \frac{\varepsilon_{r(J)} + \varepsilon_{r(J-1)}}{r_{(J)} + r_{(J-1)}} \quad \text{(I-6a)}$$

Eq. (I-6b) is the simplification of Eq. (I-6a)

$$\left[\frac{\sigma_{r(J)} + \sigma_{r(J-1)}}{2k} + \frac{E_d A_d \mathrm{Coef}}{2C}\right]^2 = \frac{m_a\sigma_c}{2}\left[\sigma_{r(J)} + \sigma_{r(J-1)}\right] - \frac{m_a\sigma_c E_d A_d}{2C}\mathrm{Coef} + s_a\sigma_c^2 \quad \text{(I-6b)}$$

Considering the Eqs. (I-7) to (I-10)

$$\begin{cases} \dfrac{r_{(J)}}{r_{(J-1)}} = \dfrac{2\varepsilon_{\theta(J-1)} - \varepsilon_{r(J-1)} - \varepsilon_{r(J)}}{2\varepsilon_{\theta(J)} - \varepsilon_{r(J-1)} - \varepsilon_{r(J)}} \\ \lambda_{(J)} = \dfrac{r(J)}{\mathrm{re}} \end{cases} \quad \text{(I-7)}$$

$$\frac{\lambda_{(J)}}{\lambda_{(J-1)}} = \frac{2\varepsilon_{\theta(J-1)} - \varepsilon_{r(J-1)} - \varepsilon_{r(J)}}{2\varepsilon_{\theta(J)} - \varepsilon_{r(J-1)} - \varepsilon_{r(J)}} \quad \text{(I-8)}$$

$$\varepsilon_{r(J-1)} + \varepsilon_{r(J)} = \frac{2\left[\lambda_{(J-1)}\varepsilon_{\theta(J-1)} - \lambda_{(J)}\varepsilon_{\theta(J)}\right]}{\lambda_{(J-1)} - \lambda_{(J)}} = \mathrm{Coef} \quad \text{(I-9)}$$

$$k = \frac{\lambda_{(J-1)} - \lambda_{(J)}}{\lambda_{(J)} + \lambda_{(J-1)}}\,,\ \mathrm{k}_1 = \frac{E_d A_d \mathrm{Coef}}{2C}\,,\ \mathrm{k}_2 = \frac{m_a\sigma_c}{4} \quad \text{(I-10)}$$

And substituting those to Eq. (I-6a) gives

$$\left[\frac{\sigma_{r(J-1)} - \sigma_{r(J)}}{2k}\right]^2 + k_1^2 + \frac{k_1}{k}\left[\sigma_{r(J-1)} - \sigma_{r(J)}\right] = 2k_2 \times \left[\sigma_{r(J)} + \sigma_{r(J-1)}\right] - 4k_1k_2 + s_a\sigma_c^2 \quad \text{(I-11)}$$

$$\rightarrow \frac{\sigma_{r(J-1)}^2}{4k^2} + \frac{\sigma_{r(J)}^2}{4k^2} - \frac{\sigma_{r(J)}\sigma_{r(J-1)}}{2k^2} + k_1^2 + \frac{k_1}{k}\sigma_{r(J-1)} - \frac{k_1}{k}\sigma_{r(J)} - 2k_2\sigma_{r(J)} - 2k_2\sigma_{r(J-1)} + 4k_1k_2 - s_a\sigma_c^2 = 0 \quad \text{(I-12)}$$

$$\rightarrow \left(\frac{1}{4k^2}\right)\sigma_{r(J)}^2 + \left(\frac{-k_1}{k} - \frac{\sigma_{r(J-1)}}{2k^2} - 2k_2\right)\sigma_{r(J)} + \left(\frac{\sigma_{r(J-1)}^2}{4k^2} + k_1^2 + \frac{k_1}{k}\sigma_{r(J-1)} - 2k_2\sigma_{r(J)} + 4k_1k_2 - s_a\sigma_c^2\right) = 0 \quad \text{(I-13)}$$

Answer of this second order equation is

$$\sigma_{r(J)} = \frac{-b - \sqrt{b^2 - 4ac}}{2a} \quad \text{(I-14)}$$

$$where\ a = \frac{1}{4k^2}\,,\ b = \frac{-k_1}{k} - \frac{\sigma_{r(J-1)}}{2k^2} - 2k_2\,, \quad \text{(I-15)}$$

$$c = \left(\frac{\sigma_{r(J-1)}^2}{4k^2} + k_1^2 + \frac{k_1}{k}\sigma_{r(J-1)} - 2k_2\sigma_{r(J)} + 4k_1k_2 - s_a\sigma_c^2\right) \quad \text{(I-16)}$$

Appendix II- Calculation of the axial stiffness of face dowel

As the pretension force is applied, the free and the anchored length of the bolt are tensioned. The equilibrium of the axial force in the anchored length is (Fig. 17)

$$T + \mathrm{dT} = T + \tau.\pi.d_b.\mathrm{dx} \quad \text{(II-1)}$$

where *T*=force in the anchored length, *db*=diameter of bolt, and τ=shear stress on reinforcement perimeter, which can be obtained by

$$\tau = \mathrm{Kini}.v \quad \text{(II-2)}$$

where *v*=relative displacement between the rock mass and the bolt, and *Kini*=initial shear stiffness between the bolt and the rock mass, expressed as (Cai *et al*. 2004)

$$K_{\mathrm{ini}} = \frac{H}{\pi \mathrm{d}_{\mathrm{rein}}} \quad \text{(II-3)}$$

where *H*=material parameter associated to the shear stiffness between the bolt and the rock mass and can be computed by Eq. (II-4)

$$\mathrm{H} = \frac{2\pi\ \mathrm{Gg}\ \mathrm{Gm}}{\left[\ln\left(\frac{R}{\mathrm{rb}}\right) - \frac{1}{2}\right]\mathrm{Gg} + \ln\left(\frac{\mathrm{rg}}{\mathrm{rb}}\right)\mathrm{Gm}} \quad \text{(II-4)}$$

where *rb* and *rg*=radius of the bolt and radius of the grout borehole; *Gg* and *Gm*=shear modulus of the grout mortar and the rock mass, respectively; and *R*=influence radius of a single rock bolt. Substituting Eq. (II-2) from Eq. (II-1) and then taking derivation gives

$$\frac{d^2T}{\mathrm{dx}^2} - \lambda^2 T = 0 \quad \text{(II-5)}$$

in which

$$\frac{\mathrm{dv}}{\mathrm{dx}} = \frac{T}{E_b A_b} \quad \text{(II-6)}$$

$$\lambda = \left(\frac{\mathrm{Kini}.\pi\mathrm{db}}{E_b A_b}\right)^{0.5} = \left(\frac{H}{E_b A_b}\right)^{0.5} \quad \text{(II-7)}$$

Ab and *Eb*=the area section and the elastic modulus of the bolt, respectively. The solution of the preceding differential equation is

$$T = C1e^{\lambda.x} + C2e^{-\lambda.x} \quad \text{(II-8)}$$

*C*1 and *C*2 are constants obtained by the following

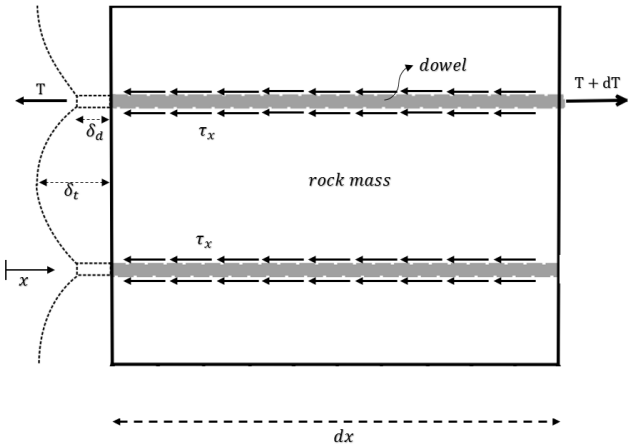

Fig. 17 Dowel and rock interaction and stress distribution

boundary conditions:

At x=0, T=0 and at x=L, v=0 gives

$$K_{\text{rein}} = \frac{H}{\lambda}\left(\frac{e^{\lambda L}+e^{-\lambda L}}{e^{\lambda L}-e^{-\lambda L}}\right) \quad \text{(II-9)}$$

$$T_{\text{modified}} = T_{\text{ideal}} - \left[-T_{\text{ideal}}\left(\frac{e^{-\lambda L}}{e^{\lambda L}+e^{-\lambda L}}\right)e^{\lambda x} - T_{\text{ideal}}\left(\frac{e^{\lambda L}}{e^{\lambda L}+e^{-\lambda L}}\right)e^{-\lambda x}\right] \quad \text{(II-10)}$$

where T_{ideal} =force on the bolt in the ideal connection between the bolt and the rock mass; force on the bolt head considered T=0.